

The evolutionary status of Sher25 - implications for blue supergiants and the progenitor of SN1987A

S. J. Smartt¹, D. J. Lennon², R. P. Kudritzki³, F. Rosales¹, R. S. I. Ryans⁴, and N. Wright¹

¹ Institute of Astronomy, University of Cambridge, Madingley Road, CB3 0HA, Cambridge, England

² The Isaac Newton Group of Telescopes, Apartado de Correos 368, E-38700, Santa Cruz de La Palma, Canary Islands, Spain

³ Institute for Astronomy, University of Hawaii at Manoa, 2680 Woodlawn Drive, Honolulu, Hawaii 96822

⁴ The Department of Pure and Applied Physics, The Queen's University of Belfast, Belfast BT7 1NN

Received 19-02-02; accepted 03-06-02

Abstract. The blue supergiant Sher25 in the massive Galactic cluster NGC3603 is surrounded by a striking emission line nebula. The nebula contains an equatorial ring and probable bi-polar outflows, and is similar in morphology, mass and kinematics to the shell now visible around SN1987A. It has been suggested that both nebulae were ejected while Sher 25 and the progenitor of SN1987A were in previous red supergiant phases. In the case of Sher 25 this is based on the qualitative strengths of nebular [N II] emission which is indicative of nitrogen enriched gas. This gas may have been dredged up to the stellar surface by convective mixing during a previous red supergiant phase. We present optical high-resolution spectra of Sher 25 and a model photosphere and unified stellar wind analysis which determines the atmospheric parameters, mass-loss rate and photospheric abundances for C, N, O, Mg, and Si. We compare these results, in particular CNO, to other Galactic B-type supergiants and find that Sher 25 does not appear extreme or abnormal in terms of its photospheric nitrogen abundance. The C/N and N/O ratios are compared to surface abundances predicted by stellar evolutionary calculations which assume the star has gone through a red supergiant phase and convective dredge-up. In particular we find that the N/O abundance is incompatible with the star having a previous red-supergiant phase, and that the nebulae is likely to have been ejected while the star was a blue supergiant. The results are compatible with some degree of rotationally induced mixing having occurred while the star was on or near the main-sequence. This is similar to what has recently been found for nebulae surrounding LBVs. In addition our wind analysis suggests the star currently has a relatively normal mass-loss rate in comparison with other Galactic B-type supergiants and sits comfortably within the wind momentum-luminosity relationship. In light of the evidence regarding massive evolved early-type stars in the Galaxy we suggest there is no object which shows any evidence of having had a previous red supergiant phase and hence of undergoing blue loops in the HR diagram.

Key words. stars: supernovae — stars: individual(Sher25) — stars: supergiants — stars: abundances — stars: winds, outflows

1. Introduction

The study of hot luminous B-type supergiant stars is of fundamental importance for understanding the late evolutionary stages of massive stars and the chemical evolution of our own and external galaxies. Massive stars enrich the interstellar medium with the heavy chemical elements during all stages of their evolution, from fast winds in their early hot stages through cool dense outflows from red supergiants and finally and most spectacularly during their deaths in core-collapse supernovae explosions. The fact that the progenitor of SN1987A was identified as a hot B-type supergiant makes them extremely interesting

objects, being the final stage in the life of at least some very massive stars.

NGC 3603 is a massive H II region ionized by a young, luminous cluster located approximately 7kpc from the Sun in the fourth galactic quadrant ($l=291^{\circ}.62$, $b=-0^{\circ}.52$). It has been described as the most massive optically visible giant H II region in the Galaxy (Goss & Radhakrishnan 1969). Given its relative proximity and the large number of massive stars it contains, this cluster provides an opportunity to study the upper mass region of the IMF and the evolutionary processes of very massive stars. It contains approximately 50 O and early B-type stars and the age of the original starburst is estimated somewhere between 2-4 Myr (Melnick et al. 1989, Moffat 1983, Crowther

& Dessart 1998). The cluster includes the trapezium-type system HD97950 which has three WR stars identified and six O3 stars all within 0.3 pc (Drissen et al. 1995). Of particular interest is the star no. 25 reported first by Sher (1965). Moffat (1983) presented a moderate resolution spectrum of this blue supergiant and classified it as a B1.5Iab and Van den Bergh (1978) has described it as the most highly evolved star in the cluster.

The main reason for the interest in this star is the spectacular circumstellar nebula, discovered by Brandner et al. (1997a) and beautifully illustrated in HST press release images STScI-PRC99-20¹. It consists of a ring-shaped equatorial emission line nebula (expansion velocity of 20 km s⁻¹) and probable bipolar outflows to the northeast and to the southwest (expansion velocity of 83 km s⁻¹). The H α + [N II] and NIR images of Brandner et al. (1997a, 1997b) indicate that both the ring and the bipolar ejecta have roughly the same dynamical age which would suggest a common origin in a stellar outburst approximately 6600 yrs ago. The [N II]/H α emission line ratio of the ring appeared to be higher than that of the background H II region, which Brandner et al. have qualitatively interpreted as evidence for nitrogen enrichment in the ejecta and hence possibly that the gas has been processed through the CN and ON-cycles in the core of Sher 25 during its main-sequence phase. However there are no *quantitative* determinations of electron temperature, density and hence abundances in either the ring or bi-polar lobes. Sher 25 is currently a hot blue supergiant and Brandner et al. have suggested that the star lived briefly for a period as a red supergiant during which time it ejected the nebula. In this picture Sher 25 has undergone a “blue-loop” in the HR diagram, first evolving to the red after main-sequence core-H exhaustion and then back again to the B-type supergiant region. However these conclusions are based mainly on the existence and morphology of the nebula and the suggestion that it may be enriched with nitrogen. How massive stars generally evolve in the upper regions of the HR diagram is still not well understood. Theoretical models have many free parameters which can affect the path of a star after (and in some cases during) the main-sequence lifetime, such as mass-loss, rotation, convection and overshooting treatment, and metallicity. Observational evidence on the evolutionary status and history of evolved massive stars such as blue and red supergiants, LBVs and WR stars provide necessary constraints on the models. Hence determining the nature of the circumstellar gas and the evolutionary phase of Sher 25 is of great interest in this context. In addition it has been suggested (by Brandner et al. 1997b) that Sher 25 could be a twin of the progenitor of SN1987A, which was a B3Ia supergiant (Walborn et al. 1989). This is due to the existence of a similar ring structure now seen around SN1987A which in existence before the SN explosion and hence was ejected by the progenitor star. Fransson et al. (1989) suggested that it had passed through a previous RSG phase

given the CNO line strengths in the early-time UV spectra, although the uncertainties are large. Therefore the star Sher 25 could be a possible supernova Type II progenitor.

In the wider picture the existence and relative number of blue supergiants in different mass ranges needs to be understood to provide stronger constraints on evolutionary theory. The problem with predicting the correct number ratio of blue-red supergiants in different metallicity regimes was first pointed out by Langer & Maeder (1995). The B/R-ratio appears to increase with metallicity and such a trend has not been generally reproduced by theory. Recently Maeder & Meynet (2001) have suggested that introducing rotation into the calculations does go some way to improving the comparison with observations. If massive stars do go through blue-loops then the blue-supergiant population may be made up of pre- and post red-supergiant objects (e.g. see models of Schaller et al. 1992). However distinguishing between two populations and determining their ratios has been a notoriously difficult problem. One method that has been tried is using stellar surface chemistry as an indicator of evolutionary status. Qualitatively for example Jaschek & Jaschek (1967) and later Walborn (1972) suggested that the carbon and nitrogen line strengths in OB stars could be used to define separate populations, which led to the OBN/OBC spectral classification. In this scheme the OBN stars generally have stronger nitrogen and weaker carbon lines, and vice-versa for the OBC stars. Also there is a wide variation in the strength of the differences found between stars. These stars are usually explained by invoking some mechanism that will mix core processed gas to the surface. This could be either dredge up by convective mixing during a previous red supergiant phase, or alternatively rotationally induced mixing during and just after the main-sequence phase could provide an efficient mechanism (e.g. Denissenkov 1994, Talon et al. 1997, Maeder & Meynet 2001).

As the nebulae around Sher 25 could be suggestive of it having definitely gone through a previous red-supergiant phase, it is of great interest to study its atmospheric and wind parameters in detail and deduce its surface chemical composition. These can then be compared with values estimated from different evolutionary scenarios, and also compared to the general population of Galactic B-type supergiants. A great deal of effort has recently been invested in understanding Galactic B-type supergiants and two papers in particular have set cornerstones in the field. The first is the non-LTE model atmosphere study of atmospheric parameters, line strengths and abundance trends of McErlean et al. (1999, hereafter Paper I), which studied a large sample of B-type supergiants in a homogeneous way. The difficulties in analysis methods and ways of mitigating errors were presented which provides an excellent starting point for future detailed analysis of single objects or homogeneous groups. The second is the extensive study of the wind parameters of fourteen early B-type supergiants by Kudritzki et al. (1999, hereafter Paper II). This used non-LTE unified model atmospheres to investigate

¹ <http://oposite.stsci.edu/pubinfo/PR/1999/20/index.html>

the $H\alpha$ line profiles and determine stellar wind properties for a subset of the stars in Paper I (and some A-type supergiants in addition). A tight relationship between the stellar wind momentum and luminosity was found, and the Balmer line profiles were quantitatively reproduced.

In this paper we present a non-LTE model photosphere analysis to deduce the surface parameters and abundances of Sher 25. In addition, a non-LTE unified model atmosphere is used to analyse the $H\alpha$ emission line and characterise the stellar wind. We place the results of these analysis in the general context of the previously analysed large sets of Galactic B-type supergiants.

2. Observational data

Spectra of Sher 25 ($V = 12.3, B = 13.7$; Brandner et al. 1997a) were taken with the UCLES échelle spectrometer at the Anglo-Australian Telescope on the night of 28th June 1999. The 79 lmm^{-1} grating and the MIT2 CCD detector were used. The CCD was of format $4\text{k}\times 2\text{k}$ with $15\mu\text{m}$ pixels, which results in a $1''$ entrance slit projecting onto four pixels on the detector. To avoid this over-sampling and increase the signal-to-noise per resolution element, we binned the CCD on readout to $2\text{k}\times 1\text{k}$. Two wavelength regions were observed, one centred on 4335\AA and the other on 6560\AA . The slit width was kept constant at $1''$, and the FWHM of the arc lines at the centres of these settings were measured at 0.11\AA and 0.17\AA respectively. One exposure of 1200s was taken in the red setting, and $4\times 1200\text{s}$ were taken in the blue; exposures of comparison arc lamps were taken immediately after each science set of exposures. The purpose of the red setting was mainly to get the $H\alpha$ profile, while the blue covers the higher lines in the Balmer series, and all of the He I and weaker metal lines required for atmospheric diagnostics. The 2D frames were bias corrected, flat-fielded, and the spectral orders were optimally extracted using standard routines within IRAF. After wavelength calibration the four blue frames were cross-correlated (taking the best S/N spectrum as a reference) to check for velocity shifts. None were found at a significance greater than the estimated error of $\sim 6 \text{ km s}^{-1}$, so the spectra were co-added. The final blue spectra had a dispersion of 0.06\AA pix^{-1} in the central order, which considerably over-samples the metal line profile widths. The mean FWHM of several of the stronger metal lines (in the region $4550\text{--}4620\text{\AA}$) was measured at 1.5\AA (98 km s^{-1}), hence the spectra were rebinned to a dispersion of 0.3\AA pix^{-1} . At the furthest useful blue wavelength (3915\AA) this corresponds to 4 resolution elements sampling the FWHM which is adequate for line profile fitting and significantly increased the S/N in the continuum. The MIT2 CCD is too large for the window of the UCLES camera, hence the ends of each échelle order are severely vignetted. The ends of each order were thus trimmed, and the final useful spectrum has almost complete coverage of $3915\text{--}5280\text{\AA}$ across 15 orders, with gaps of $5\text{--}15\text{\AA}$ appearing only between the last 5. The signal-noise-ratio ranges

between 50 at the edge orders to 70 in the central few orders.

The spectra were normalised by fitting cubic splines to continuum regions free from absorption lines in IRAF and afterwards were transferred to STARLINK spectral analysis program DIPSO (Howarth et al. 1998). The equivalent widths of the metal lines and non-diffuse lines of neutral helium were measured by the non-linear least squares fitting of single or multiple Gaussian profiles to the normalised spectra. The hydrogen and diffuse helium lines were not measured in this manner, but the normalised profiles were extracted directly for comparison with Galactic standards and with theoretical profiles.

In order to compare the atmospheric parameters, photospheric abundances and wind parameters with other typical B-type supergiants, three bright stars of similar spectral type (lying within the solar neighbourhood) were chosen as comparison standards. These were HD2905, HD 14956 and HD 13854, which have very similar $\text{He}\epsilon, \delta, \gamma$ lines and Si IV/Si III line strength ratios as Sher 25. These stars have been observed with the single-order spectrograph ISIS on the WHT, and the spectra have a coverage of $3900\text{--}4735\text{\AA}$ covering the main diagnostic lines of interest (see Smartt et al. 2001 where the details of the instrument setup is described). The S/N of these spectra are very high (in excess of 200) and the line profiles are well resolved, hence they make excellent comparison templates. Equivalent widths for these stars were also measured in a similar method described above. These three stars were also part of the Lennon et al. (1993) atlas, which covers the region $3950\text{--}5000\text{\AA}$, and the $H\alpha$ region $6260\text{--}6870\text{\AA}$. Line strength measurements in wavelength regions not covered by the WHT ISIS spectra (mainly $4735\text{--}5000\text{\AA}$) were taken from this source. The final values of equivalent widths for each star can be found in Table 2.

Table 2. The atmospheric parameters derived for Sher 25 and the three comparison supergiants, with the homogeneous method described in Sect.3.

Star	T_{eff} (K)	$\log g$ (cgs)	$v_{\text{turb}}^{\text{Si}}$ (kms^{-1})	$v \sin i$ (kms^{-1})
Sher 25	$22\,300 \pm 1000$	2.60 ± 0.1	15 ± 5	65
HD2905	$23\,500 \pm 1000$	2.70 ± 0.1	11 ± 5	80
HD13854	$22\,000 \pm 1000$	2.65 ± 0.1	13 ± 5	80
HD14956	$21\,250 \pm 1000$	2.55 ± 0.1	12 ± 5	75

3. Model atmosphere and wind analysis

3.1. Photospheric analysis and abundances

The photosphere of Sher 25, and subsequently the three comparison stars, were modeled using the techniques described in detail in Paper I and briefly summarized in Smartt et al. (2001a). A grid of non-LTE model atmospheres has previously been generated using the code

Table 1. Equivalent widths for metal lines of Sher 25 and comparison stars given in mÅ units.

Ion and Line	HD2905	HD13854	HD14956	Sher 25
C II 4267.02 & 4267.27	111	155	128	125
C II 6578.10	...	135	105	110
N II 3995.00	101	308	443	484
N II 4035.08	25	89	101	95
N II 4236.86 & 4236.98	28	78	63	75
N II 4241.18 & 4241.78	53	119	88	165
N II 4447.03	70	106	172	134
N II 4607.16	21	134	247	265
N II 4613.87	16	91	188	160
N II 4630.54	79	301	456	398
N II 4803.29	...	122	187	107
O II 4069.62 & 4069.89	249	235	171	167
O II 4072.16	213	220	190	122
O II 4075.86	235	241	204	181
O II 4132.80	85	81	63	65
O II 4317.14	204	192	135	177
O II 4319.63 & 4319.93	205	210	155	210
O II 4345.56	264	202	147	184
O II 4347.42	...	112	77	91
O II 4349.43	397	347	267	297
O II 4351.26 & 4351.50	183	127	85	103
O II 4366.89	236	217	170	235
O II 4414.90	303	338	257	291
O II 4416.97	240	270	211	185
O II 4590.97	207	173	147	170
O II 4595.96 & 4596.18	177	137	159	134
O II 4638.86	242	212	126	159
O II 4661.63	259	233	202	194
O II 4673.74	88	57	53	60
O II 4676.24	234	222	150	253
Mg II 4481.13 & 4481.33	170	244	233	205
Si IV 4116.10	202	141	111	218
Si III 4552.62	397	455	485	555
Si III 4568.28	348	390	438	437
Si III 4575.22	219	241	293	266
Si III 4813.30	50	65	55	49
Si III 4819.72	80	90	100	96
Si III 4829.96	...	90	85	91
S III 4361.53	206	50	60	119

TLUSTY (Hubeny 1988) covering an effective temperature range $10\,000 \leq T_{\text{eff}} \leq 35\,000$ and gravities from $\log g = 4.5$ to the Eddington stability limit at each T_{eff} . Increments were 2500 K and 0.25 dex in T_{eff} and

$\log g$ respectively. Models were calculated for two helium fractions, i.e. $y = 0.09$, and $y = 0.20$, where $y = N[\text{He}]/N[\text{H} + \text{He}]$. The models contain only H and He and assume a plane-parallel atmosphere which is in hy-

Table 3. Chemical abundances calculated in the model atmosphere analysis for Sher 25 and the comparison stars. The absolute abundance derived for each line in each star is given, and also the differential abundance of Sher 25 minus each comparison star.

Element/Ion	Wavelength Å	HD2905	HD 13854	HD 14956	Sher 25	Differential Abundance of Sher 25 with respect to		
						HD2905	HD 13854	HD 14956
C II	4267.02	7.05	7.27	7.11	7.07	+0.02	-0.20	-0.04
	& 4267.27							
C II	6578.10	...	7.12	6.66	6.95	...	-0.17	+0.29
N II	3995.00	7.00	7.93	8.61	8.19	+1.19	+0.26	-0.42
N II	4035.08	7.71	8.32	8.51	8.40	+0.69	+0.08	-0.11
N II	4236.98	7.31	7.86	7.78	7.84	+0.53	-0.02	+0.06
N II	4241.18	7.64	8.07	7.93	8.28	+0.64	+0.21	+0.35
	& 4241.78							
N II	4447.03	7.20	7.53	7.98	7.45	+0.25	-0.08	-0.53
N II	4607.16	7.04	8.19	9.15	8.91	+1.87	+0.72	-0.24
N II	4613.87	7.04	8.02	8.90	8.45	+1.41	+0.43	-0.45
N II	4630.54	7.10	8.31	9.42	8.53	+1.43	+0.22	-0.89
O II	4069.62	8.95	8.91	8.65	8.39	-0.56	-0.52	-0.26
	& 4069.89							
O II	4072.16	9.03	9.10	9.03	8.20	-0.83	-0.90	-0.83
O II	4075.86	8.99	8.98	8.88	8.37	-0.62	-0.61	-0.51
O II	4132.80	9.04	9.03	8.93	8.78	-0.24	-0.25	-0.15
O II	4153.30	...	9.29	8.95	8.95	...	-0.33	+0.00
O II	4317.14	9.13	9.06	8.76	8.87	-0.26	-0.19	+0.00
O II	4319.63	9.06	9.12	8.87	8.91	-0.15	-0.21	+0.04
	& 4319.93							
O II	4366.89	9.22	9.08	8.90	8.97	-0.25	-0.11	+0.07
O II	4590.97	9.28	9.04	9.03	8.88	-0.40	-0.16	-0.15
O II	4595.96	9.19	8.91	9.24	8.80	-0.39	-0.11	-0.44
	& 4596.18							
O II	4638.86	9.44	9.45	9.19	9.37	-0.07	-0.08	+0.18
O II	4661.63	9.35	9.21	9.17	8.75	-0.60	-0.46	-0.42
O II	4673.74	9.13	8.83	8.86	8.80	-0.33	-0.03	-0.06
O II	4676.24	9.28	9.23	8.85	8.95	-0.33	-0.28	+0.10
Mg II	4481.13	7.44	7.58	7.54	7.46	-0.02	-0.12	-0.08
	& 4481.33							
Si III	4552.62	7.90	8.00	8.43	8.17	+0.27	+0.17	-0.26
Si III	4568.28	7.93	7.97	8.50	8.00	+0.07	+0.03	-0.50
Si III	4575.22	7.88	7.87	8.40	7.92	+0.04	+0.05	-0.48
Si III	4813.30	7.35	7.45	7.49	7.28	-0.07	-0.17	-0.21
Si III	4819.72	7.46	7.54	7.81	7.54	+0.08	+0.00	-0.27
Si III	4829.96	...	7.40	7.53	7.37	...	-0.03	-0.16
Si IV	4116.10	7.22	7.41	7.56	7.43	+0.21	+0.02	-0.13

drostatic equilibrium. The consequences of these assumptions have been discussed in Paper I. Line formation calculations for all the ionic species with absorption lines observed in the spectra of Sher 25 were calculated using the codes DETAIL (Giddings 1981), and SURFACE (Butler 1984). Microturbulence was included in the calculations

as an extra free parameter, and the statistical equilibrium calculations were performed for the species H I, He I, C II, N II, O II, Si III, Si IV and Mg II. The atomic data employed were identical to those used in Paper I.

Although the photospheric analysis is based on NLTE atmospheres, they are plane-parallel and do not account

Table 4. The mean of the individual line abundances from Table 3 for each element in each star. Also listed is the mean of the differential results. The absolute values are quoted on the logarithmic scale $12 + \log[N_x]/[N_H]$ (see Sect. 3.1.2). The mean abundances were determined by first determining the fractional abundance $[N_x]/[N_H]$ for each line, calculating the linear mean and quoting this on the original logarithmic scale. The errors quoted are the standard errors in the mean (σ/\sqrt{n}); where n is the number of features used, and σ is the standard deviation of the sample again calculated on a linear scale. These represent the statistical scatter of the measurements, however a further systematic error will be present in each case.

Ion	HD2905	HD13854	HD 14956	Sher 25	Differential Abundance of		
					Sher 25 with respect to		
					HD2905	HD 13854	HD 14956
C II	7.05	7.20±0.07	6.94±0.17	7.01±0.06	+0.02	-0.18±0.01	+0.16 ±0.13
N II	7.34±0.10	8.09±0.07	8.70±0.13	8.42±0.12	+1.29±0.16	+0.30±0.10	-0.13 ±0.12
O II	9.18±0.14	9.12±0.05	8.98±0.04	8.87±0.07	-0.34±0.16	-0.25±0.05	-0.10 ±0.06
Mg II	7.44	7.58	7.54	7.46	-0.02	-0.12	-0.08
Si III	7.41±0.05	7.47±0.04	7.63±0.10	7.41±0.07	-0.00±0.05	-0.06±0.05	-0.21 ±0.03
Si IV	7.22	7.41	7.56	7.43	+0.21	+0.02	-0.13

for metal line blanketing or wind contamination. In this paper we concentrate on differential abundance determinations and comparing stars of similar atmospheric parameters, and acknowledge that the absence of these physical effects in our models may compromise the final absolute abundances. In the future it is our desire to pursue a fully unified model atmosphere and wind analysis of sher25 with even higher quality spectral data from, for example, the UVES spectrometer on the VLT. This would allow an excellent comparison between the very weak metal lines formed deep in the photosphere, and the stronger lines we see in the current ucles spectra.

3.1.1. Determination of atmospheric parameters

The relative strengths of two ionization stages of silicon can be used to determine the effective temperature for stars of early-B spectral types. Absorption lines of Si III and Si IV are well observed and reliably measured in the UCLES spectra of Sher 25. The line strengths are listed in Table 1, with six lines of Si III and one of Si IV initially used to determine T_{eff} . There is an inherent problem in DETAIL when calculating the Si III line strengths of the 4552Å triplet, which has been discussed in Paper I. In the lowest gravity models having effective temperatures of 22 500K or higher, DETAIL calculations showed an overpopulation of the upper levels of Si III in atmospheric regions where the lines are formed. This is particularly problematic for the 4552Å triplet but is less pronounced for the 4813Å triplet which is formed deeper in the atmosphere. The effect leads to a filling-in of the 4552Å multiplet line profiles, and hence one needs to increase the Si abundance substantially to offset this effect. One can readily see this in Table 3, where the mean abundances derived from the 4552Å triplet are between 0.5–0.8 dex higher than those derived from 4813Å. We follow the conclusion in Paper I that the 4552Å lines are not reliably modeled with our

methods and use only the 4813Å triplet in determining the effective temperature of all four stars.

The shape of the Balmer line profiles (H ϵ , H δ and H γ , and H β) are useful indicators of the stellar surface gravity. In particular the width of the line wings are excellent indicators of $\log g$. Assuming an initial T_{eff} , the surface gravity is calculated by fitting the observed profiles with theoretical lines calculated at different values of $\log g$, paying particular attention to the line wings. The mean of the results from H δ and H γ was used. H ϵ suffers from interstellar contamination (Ca II) and a stellar blend with He I. Both H β and H α can show significant emission contributions from the stellar wind and the latter is discussed in Sect. 3.2. Some iteration in the simultaneous determination of T_{eff} and $\log g$ was necessary, given the interdependence of each parameter but convergence was normally achieved within 3-4 cycles.

The microturbulent velocity was estimated by requiring that each line of the Si III triplet at 4552Å gave the same abundance. The determination of v_{turb} in this way has been discussed in Paper I and it has the advantage that three lines from the same multiplet with quite different equivalent widths are used. The lines of O II can also be used and these often give higher values compared to those derived when using Si III. Due to the homogeneity of the atomic data and the large range in line strengths covered, we use the value derived from the Si lines, and note that as we re-derive all parameters for the standards (and subsequent abundances) in a homogeneous way any systematic error in this procedure will be mirrored in Sher 25 and the three comparison stars.

The three parameters of T_{eff} , $\log g$ and v_{turb} were varied so that a simultaneous fit to all three was achieved for Sher 25, and the final atmospheric parameters are listed in Table 2. The $v \sin i$ of the star was determined by convolving the theoretical line profiles of prominent metal lines with a rotational broadening function until good agreement with the observed profile was achieved (as discussed

in Lennon et al. 1991). We then chose three stars which had very similar atmospheric parameters from the list of bright nearby B-type supergiants analysed in Paper I. Two stars of almost identical T_{eff} are HD14956 and HD13854, and the observed profiles of the hydrogen and helium lines were compared directly to make sure the luminosity class and the helium line strengths (and hence the atmospheric helium composition) were indeed very similar. This can be seen in Figs. 3.1.1 and 3.1.1. A third star HD2905 was also chosen as an extra comparison due to its relatively weak nitrogen line spectra, hence giving us comparison stars which are both qualitatively nitrogen rich and poor.

Using the higher quality spectra now available to us (as described in Sect. 2) we have re-derived the atmospheric parameters of the comparison stars using identical methods to that used for Sher 25. Our results for HD 2905 and HD 14956 are identical to those in Paper I, however we derive a T_{eff} which is 1500 K cooler than the previous analysis for HD 13854. The reason for this is likely to be the slightly different equivalent widths of the Si IV 4116 Å line measured in each study. We measure this line as having a strength of 111 mÅ and it is quoted as 160 mÅ in the spectra of Lennon et al. (1993). In order to keep this analysis as consistent as possible we use our refined temperature, which is similar to the previous result in Paper I within the quoted errors. The line profiles and strengths of the He I lines were all similar in Sher 25 and the 3 comparisons (as seen in Fig. 3.1.1). This suggests a very similar He abundance across the four stars within the expected uncertainties however there is difficulty in modeling all the singlet and triplet lines simultaneously and satisfactorily (see Paper I). The lines which appear to be modeled satisfactorily are the singlets He I 4437 Å and 4387 Å which form deepest in the atmosphere. However the 4437 Å line falls on top of the diffuse interstellar band at 4430 Å which is particularly strong in the Sher 25 sight line, and does not allow accurate extraction of the stellar line. The 4387 Å line in Sher 25 gives a helium fraction $y = 0.1 \pm 0.02$, hence there is no evidence of a He overabundance. The 4471 Å line, being a triplet, is difficult to model in quantitative terms but the similarity in the empirical spectra of all four supergiants, and a measured equivalent width of 820 Å (compare with Fig. 3 in Paper I) suggests that there is no evidence for using a non-solar He value in the Sher 25 model atmospheres and that all four stars have comparable He abundances.

3.1.2. Photospheric abundances

The atmospheric parameters were used to define final model photospheres for all four stars. All unblended metal-line absorption features identified in Sher 25 (and the same features in the other stars) were modeled using the line formation codes DETAIL and SURFACE as described in Sect. 3.1.1. A curve of growth method was used to determine an ionic abundance for each line, and the results are quoted on the scale $12 + \log[N_x]/[N_H]$ where N_x and

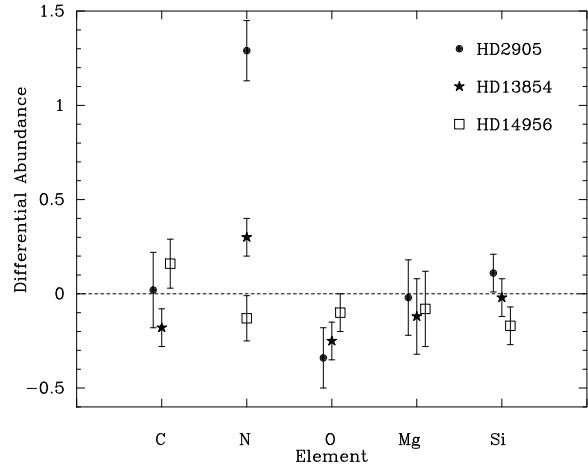


Fig. 3. Differential abundance of Sher 25 with respect to HD2905, HD14956 and HD13854. The values and errors are taken from Table 4, with the minimum error assumed to be 0.1 dex.

N_H are the abundance of ion x and hydrogen by number (see Table 3). The mean of all the individual lines were calculated, by first determining N_x/N_H , calculating the mean and then converting back to the logarithmic scale. Standard deviations (σ) and standard errors in the mean (σ/\sqrt{n} ; where n is the number of features used) were calculated and are quoted in Table 4. The differential abundance of Sher 25 with respect to each comparison star was done on a line-by-line basis and the mean values of these results were calculated in a similar way. These results should be more reliable than the absolute abundances as the differential approach mitigates the uncertainties in the atomic data and physical methods. We discuss the results for each element briefly below, and the implications of these will be discussed in Sect. 4.

Carbon: The carbon abundance is based on two lines only, being the only reliably measured features in the Sher 25 spectrum. There is a C II doublet at 6578.10 Å and 6582.85 Å, however the latter is contaminated by the nebular [N II] 6583.6 Å line. There is quite strong nebulosity around Sher 25 which was clearly visible on the raw 2D CCD images, and perfect subtraction of the features was not possible during data reduction. Hence the 6582.85 Å line of C II was not usable, although it is reliably measured in the bright comparison stars. The 4267 Å doublet is well known to give unreliable absolute abundances with the particular line formation codes we have used (e.g. Vrancken et al. 2000, Lennon 1983, Paper I), hence the values from this feature should be treated with considerable caution. Even in B-type dwarfs this line has historically proved difficult to model reliably (in either LTE or NLTE) and Sigut (1996) suggests that the model atom of Eber & Butler (1988) which we have employed needs extension to improve results from this line. The differential abundances should be more reliable, and indicate that there appears little difference, within the errors, in the carbon abun-

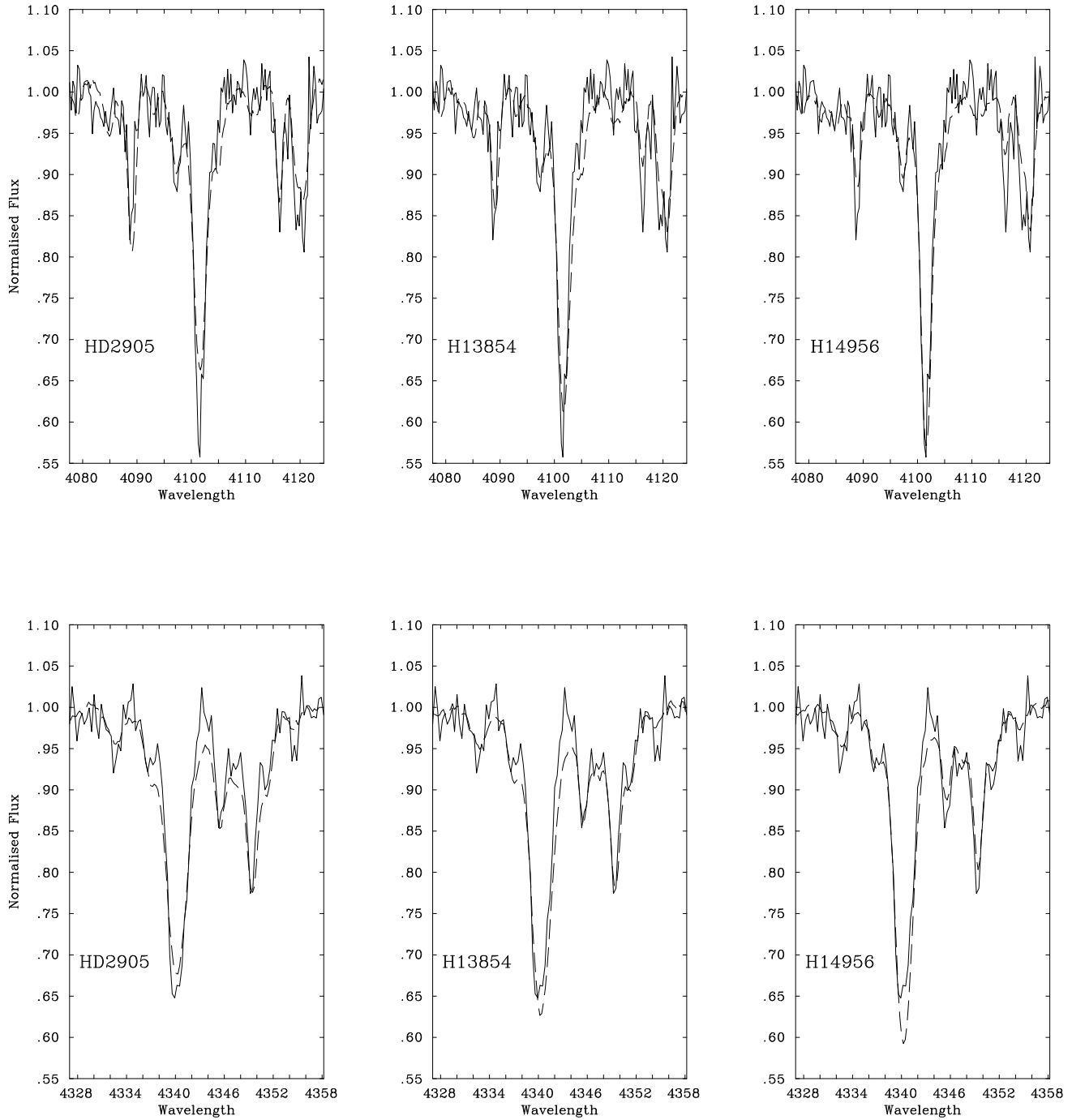


Fig. 1. The Balmer line profiles of H δ and H γ for Sher 25 and the three comparison stars. In each case the Sher 25 spectrum is the solid line, and the dashed profile is that from the three stars as labeled in each panel.

dance in the four stars. The absolute abundance derived in all four stars is very low compared to values derived in solar neighbourhood B-type stars e.g. 8.2 from Kilian (1992) and Gies & Lambert (1992) which suggests that our absolute values cannot be relied upon to be used as a quantitative test of evolutionary models (see Sect. 4). The

only other line in common with all stars (6578Å) gives similar results to 4267Å, but Paper I found that this was only satisfactorily modeled at temperatures below 20000K, and that the hotter models have this line in emission. Hence with our current codes, we do not have a good measure of the absolute carbon abundance in these stars, although

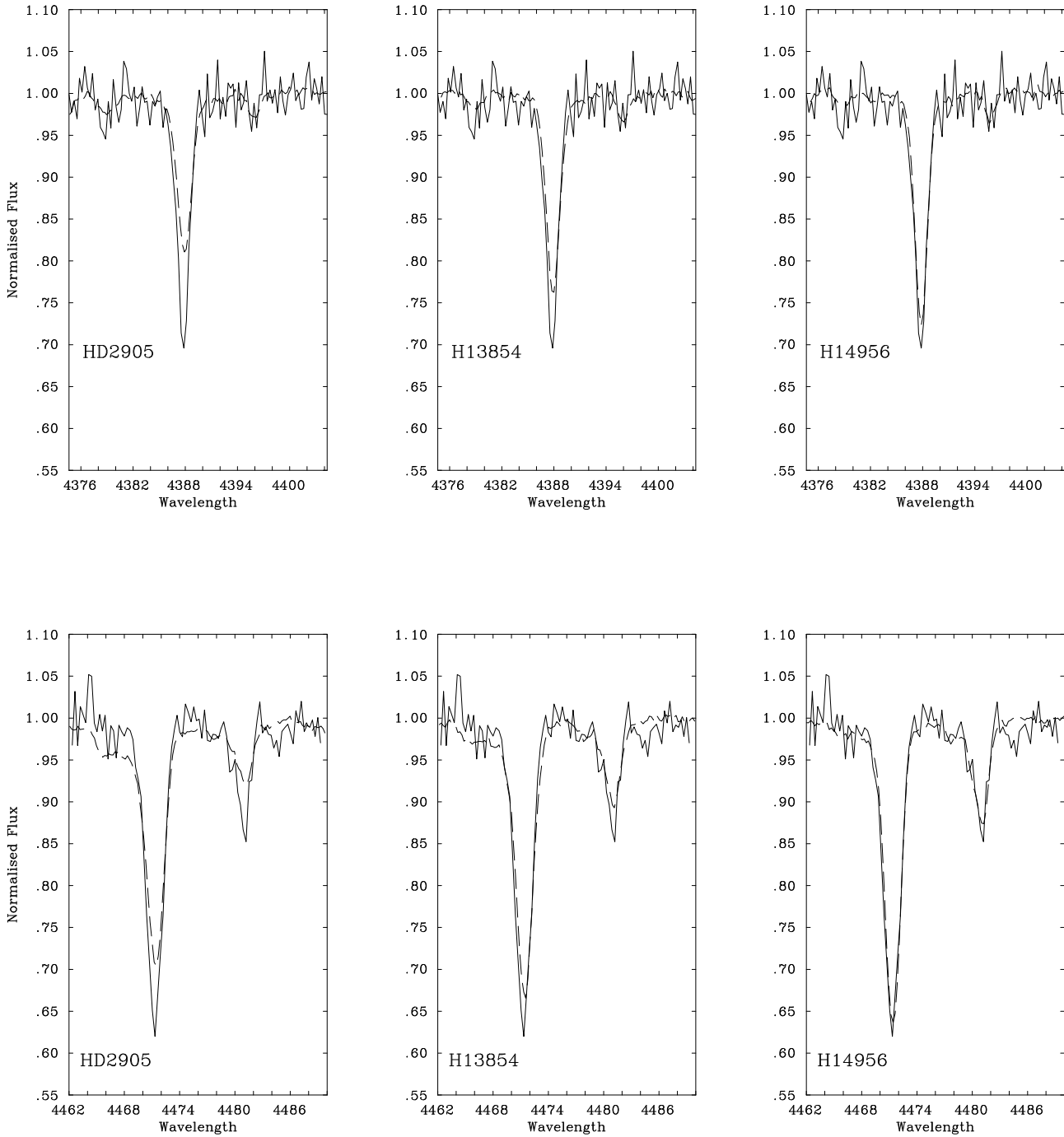


Fig. 2. The line profiles of He I 4471 Å and He I 4387 Å for Sher 25 and the three comparison stars. In each case the Sher 25 spectrum is the solid line, and the dashed profile is that from the three stars as labeled in each panel.

we can say that the abundances appear fairly similar in each atmosphere.

Nitrogen: Eight lines of N II were identified and measured in Sher 25 and each were found in the comparison stars, hence giving a good measurement of the nitrogen abundance in statistical terms. As expected, the nitrogen

abundance in HD2905 is much lower than in either of the other two comparison stars and in Sher 25. This star has very weak N II absorption features and has been classified as a BC0.7Ia (Lennon et al. 1992). This star was chosen as a comparison to show the difference between the nearby B-type supergiants that is observed. The nitrogen abun-

Table 5. The errors listed in this table illustrate how the abundances in Sher 25 would vary within the error bars of the atmospheric parameters. The values were calculated around the model atmosphere with $\log g = 2.6$, $T_{eff} = 22\,300$, $\xi = 15\text{ km s}^{-1}$. The final column lists the total error estimated by adding the individual errors in quadrature.

Species	$\log g \pm 0.2$	$T_{eff} \pm 1\,000$	$\xi \pm 5$	$\Delta \log E/H$
C II	± 0.03	± 0.02	± 0.06	± 0.07
N II	± 0.18	± 0.10	± 0.27	± 0.34
O II	± 0.13	± 0.15	± 0.18	± 0.18
Mg II	± 0.27	± 0.15	± 0.11	± 0.33
Si III	± 0.18	± 0.10	± 0.10	± 0.23

dance in Sher25 is much greater than in HD2905, and is intermediate between the other two stars (illustrated in Fig 3). Paper I indicates that at the T_{eff} of our stars, the N II line strengths in the bulk of the stars are reasonably well modeled with a “normal” nitrogen abundance of 7.7 dex. Problems with overpopulation of upper atomic levels and emission features appearing in line profiles were not in evidence for N II in this temperature regime, unlike C II and Si III. Hence we have more confidence in using the absolute values of N II as being useful for quantitative comparisons with evolutionary calculations discussed in Sect. 4.

Oxygen, magnesium and silicon: With fourteen lines measured in Sher25 oxygen is the best sampled element, as is normal in early B-type stars. Paper I found that the O II absolute abundances in this temperature range did not suffer any obvious problems with high photoionization rates. Given the good statistical sample of O II features, and the encouraging analysis in Paper I we assume that the oxygen abundance derived in our stars is reliable enough to use in comparison with evolutionary calculations. There is some evidence that the oxygen abundance in Sher25 is somewhat lower than in the three standard stars, in particular in comparison with HD2905 and is discussed in Section 4 below where we consider the implications of CNO processing in these objects. Both magnesium and silicon in Sher25 are very similar to the abundances derived in the standard stars. As these two elements should not be affected by any mixing or dredge-up processes that may affect the CNO surface composition, the fact that they are similar in all three stars points towards them all having fairly similar initial chemical compositions.

3.2. Stellar wind analysis

As the origin of the gas surrounding Sher25 is a key factor in the evolutionary history of this object, an investigation of the stellar wind properties is highly desirable. Further we can compare results directly with the extensive study of Paper II (Kudritzki et al. 1999) which investigated the wind properties of 14 Galactic early B-type

supergiants. The method used to determine the mass-loss rate for Sher25 is described in detail in Paper II. Exactly the same code is used in this case (Santolaya-Rey et al. 1997) and here we briefly outline the procedure used.

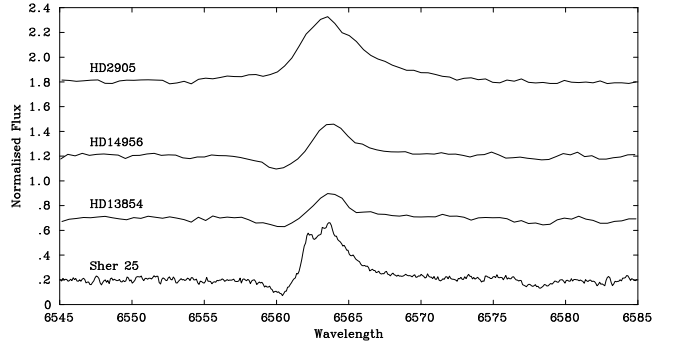


Fig. 4. The $H\alpha$ profiles of Sher25 and the three comparison stars. The secondary emission peak bluewards of the rest wavelength of $H\alpha$ in Sher25 is due to imperfect nebular subtraction in the 2D image. Weak residuals of the [N II] 6583.6Å & 6548.1Å nebular lines can also be seen. The $H\alpha$ emission of Sher25 is similar in strength to the comparison stars and the wind analysis implies it has quite normal mass-loss

The stellar parameters determined above were used to calculate the emergent flux from a non-LTE model atmosphere, and by assuming an absolute visual magnitude of the star, a radius can be determined. However the calculation of absolute V-band magnitude depends on our knowledge of distance and reddening. The former has been calculated by several authors, the most recent of which is 6.3 ± 0.6 kpc (Pandey et al. 2000). Sher25 has $B-V = 1.4$, which indicates an extinction $E(B-V) = 1.6$ from the intrinsic colours of Deutschman et al. (1976). Pandey et al. also determine R (the ratio of total to selective reddening) towards NGC3603 and suggest a value of 4.3, which is much higher than the normal Galactic line of sight value $R = 3.1$ (Seaton 1979). However this may be applicable more towards the central regions of the cluster, whereas Sher25 sits outside the main body of young O-stars. We experimented with the value of 4.3 and determined what effect it would have on the derived intrinsic luminosity of the star and its radius and whether this was consistent with the observed $H\alpha$ profile. Assuming $R = 4.3$ would imply a luminosity of $\log L/L_{\odot} = 6.2$, and a radius of $80R_{\odot}$. These values suggest the star would be more luminous and have a larger radius than HD190603 (Paper I, Lennon et al. 1992), but the surface gravity of Sher25 we derive is incompatible with a very low gravity, extremely high luminosity star. HD190603 is probably the most luminous star in the Paper I sample, and shows $H\alpha$ very strongly in emission. Sher25 has weaker $H\alpha$ emission and broader absorption wings in the other Balmer lines, which strongly suggests it is a lower luminosity object. Also a luminosity of 6.2 would suggest that Sher25 is much more luminous,

and hence has a much lower surface gravity than either of HD2905 or HD13854, both of which have undergone a wind analysis in Paper II. However the $H\alpha$ emission line in Sher 25 is not significantly stronger than in either of the latter two, and the Balmer line profiles do not suggest a much lower surface gravity. Adopting a value of $R=4.3$ would lead to serious inconsistencies between the luminosity of Sher 25 and its spectral properties, hence it is very unlikely that such a high value of R is applicable. There does appear to be evidence for a variation in R toward this sight line, and we adopt a value of $R=3.7$ as being indicative of the true value with a probable error of ± 0.5 . With this value we obtain a radius of $59 \pm 15 R_{\odot}$. The observed $H\alpha$ profiles of the stars are shown in Fig.4. The emission peak on the blue wing of Sher 25 is indicative of imperfect nebular subtraction, however the rest of the profile will not be affected given its width and the narrow nature of the nebular line. Crowther & Dessart (1998) have also derived a distance to NGC3603 based on the absolute magnitudes of O-stars. They find a distance of 10.1 kpc, using the standard value $R=3.1$. We find that Using these numbers puts luminosity and radius of Sher 25 at very similar values to those derived using $d=6.3$ kpc and $R=3.7$ i.e. $59 \pm 15 R_{\odot}$ and $\log L/L_{\odot} = 5.9 \pm 0.2$.

No UV spectra exist to determine a terminal velocity for the wind of Sher25 we adopt a value of 1000 km s^{-1} . The values of v_{∞} for HD2905 and HD13854 are derived in Paper II and values of 1100 and 1000 km s^{-1} were found, indicating our adopted value for Sher 25 is reasonable. The mass-loss rate \dot{M} can be obtained from fitting the $H\alpha$ profile, using the non-LTE unified model atmosphere technique incorporating the stellar wind and spherical extension, as described in Paper II. A grid of models was calculated with different mass-loss rates and the best fit was found for $1.75 \times 10^{-6} M_{\odot} \text{ yr}^{-1}$, and $\beta = 1.5$ (see Fig. 5). The mass-loss rate is close to (and roughly intermediate between) the values for HD13854 and HD2950 in Paper II, and appears fairly typical for early-B supergiant stars with solar-type chemical compositions. The fit to the emission profile is good, but the absorption dip blueward of the peak is not reproduced. This dip is also seen in other early B-types of similar atmospheric parameters and mass-loss rates, and the failure of the wind analysis calculations to match the observed shape is discussed in Paper II. It may be due to the neglect of metal-line blanketing in the models, or wind variations and deviations from spherical symmetry. We further derive a luminosity of $\log L/L_{\odot} = 5.9 \pm 0.2$, and a modified wind momentum of $\log(\dot{M}v_{\infty}(R/R_{\odot})^{0.5}) = 28.9 \pm 0.3$, which would place the star close to the wind momentum-luminosity relationship for solar metallicity early B-type stars (see Paper II). Hence the most important conclusion from the fitting of the $H\alpha$ and derivation of its wind and luminosity properties is that the wind of Sher 25 looks fairly typical for an early B-type supergiant.

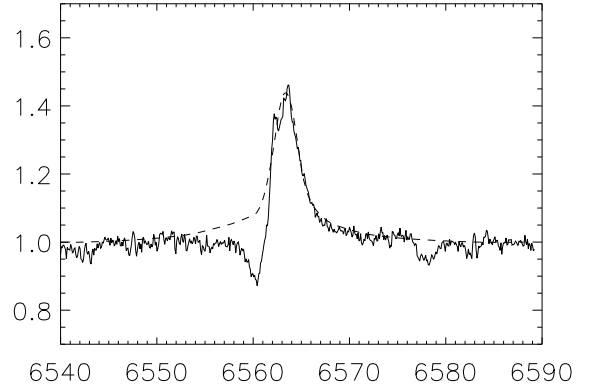


Fig. 5. The $H\alpha$ profile of Sher25 and the fit from the unified wind models. The peak is well reproduced, whereas the bluewards absorption is not seen in our model spectra due to the reasons described in Sect.3.2

4. Discussion of the evolutionary scenarios for Sher 25

4.1. A post red-supergiant star in a “blue-loop”

The existence of the ring shaped nebula and bi-polar outflow around Sher 25 has been interpreted by Brandner et al. (1997a, 1997b) as arising during a previous red supergiant evolutionary phase. In this scenario the star began its life as an O-type main-sequence object, burning H to He through the CN and the ON-cycles. After core hydrogen exhaustion, this evolutionary picture involves the star moving quickly across the HR diagram to the red supergiant region where it undergoes core He burning. During the red supergiant phase the stellar envelope becomes fully convective, which would mix a certain amount of the core material into the envelope. The relative abundances of CNO in the red supergiant atmosphere would then change drastically. The predicted final ratios of these elements will clearly depend on the mass of CN and ON-cycled core gas which is mixed into the envelope (assumed to have the stars natal composition), and the mass of the envelope which is left at the beginning of the red supergiant phase. The envelope mass will be affected by the amount of mass the star has lost during its hot main-sequence phase through radiatively driven winds. This global picture is simply and clearly described in Lamers et al. (2001). A single major mass-loss event is then invoked to explain the nebula and this dense, cool gas should have a chemical composition similar to the polluted red-supergiant atmosphere. Hence the abundances in the ionized nebula around Sher 25 could be used to test the validity of this argument, however there has been no accurate determination of abundances in the nebula to date. The spectra presented by Brandner et al. (1997a and 1997b) does not have enough wavelength coverage to estimate electron densities and temperatures consistently, hence no quantitative

Table 6. Comparison of CNO abundances from our analysis of the four B-type supergiants. For comparison the values for solar neighbourhood B-type main-sequence stars are taken from Gies & Lambert (1992), and the solar values are from Grevesse & Sauval 1998. The C, N and O element abundances are by number fraction. The numbers in italics should be treated with extreme caution, given the uncertainty in the absolute C abundance as discussed in Sect.3.1.2.

Element	Solar	B-stars	HD2905	HD13854	HD14956	Sher 25
Element abundance by number ($\times 10^{-3}$)						
C	0.33	0.16	<i>0.01</i>	<i>0.02</i>	<i>0.01</i>	<i>0.01</i>
N	0.08	0.07	0.02	0.12	0.50	0.26
O	0.68	0.48	1.51	1.32	0.95	0.74
$\frac{C+N+O}{H+He}$	0.99	0.65	1.41	1.33	1.33	0.92
Elemental fractions						
N/C	0.25	0.41	<i>2.0</i>	<i>7.7</i>	<i>55.7</i>	<i>26.3</i>
N/O	0.12	0.14	0.02	0.09	0.53	0.36

nebular abundances can be derived. These spectra do indicate that the $[N\text{II}]/H\alpha$ line strength ratio is somewhat higher than the background H II region, which Brandner et al. interpret as a sign of real nitrogen enhancement in the circumstellar gas, however a full and accurate nebular analysis is still required. After a short period as a red supergiant, and after the mass-loss has occurred it has been speculated that Sher 25 (and other blue supergiants) return to the blue region of the HR diagram, undergoing what have been called “blue-loops”.

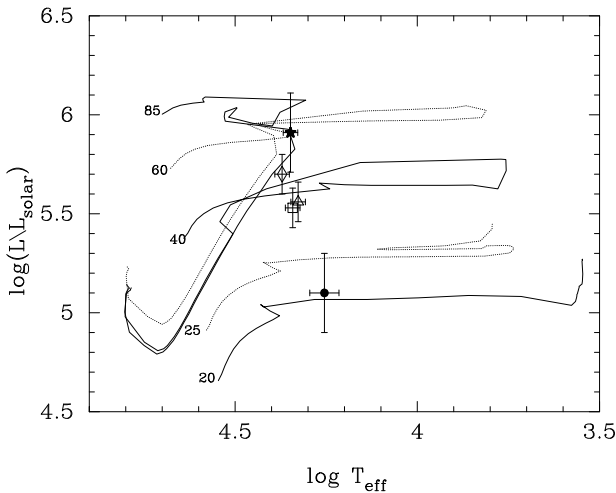


Fig. 6. Stellar evolutionary tracks for stars with zero-age main sequence masses of 20, 25, 40, 60 and $85M_{\odot}$ from Meynet et al. 1994. The symbols are Sher 25 (filled star), Sk-69°202 progenitor of SN1987A (filled circle), HD2905 (open diamond), HD13854 (open square), HD14956 (open triangle). Luminosities are taken from Paper II and Walborn et al. (1989); apart from HD13854 which was calculated assuming membership of Per OB1, distance as in Paper II, and optical magnitudes from the Simbad database.

We can use the photospheric abundances we have derived for Sher 25 to test this model of a mass-loss event

occurring when the star was a red supergiant and subsequent bluewards evolution. Lamers et al. (2001) have recently presented comparisons between chemical abundances in LBV nebulae and what one would expect in different evolutionary scenarios. They come to the conclusion that LBV nebulae are ejected during the blue supergiant phase, and that such stars have *not* gone through a previous red supergiant episode. We follow their line of argument to determine if the CNO abundances we derive in Sher 25 are consistent with a previous red supergiant phase. The Si and Mg abundances in Sher 25 are very similar to those in the three solar neighbourhood comparison stars, and these are not expected to be affected by any mixing of H-burning products into the photosphere. The Galactocentric distance of NGC3603 is approximately 8.5 kpc, roughly the same as the Sun, and galactic abundance gradients derived in Rolleston et al. (2000) and Smartt & Rolleston (1997) indicate that there is fairly low scatter in stellar metallicity at this distance from the Galactic centre. Hence we assume that Sher 25 had an initial chemical composition similar to B-type stars and nebulae in the solar neighbourhood. Table 6 lists the number fractions of CNO derived in Sher 25, the three comparison supergiants, the Sun, and solar neighbourhood B-type stars. From Table 6 and Table 4 it is apparent that Sher 25 has a nitrogen abundance approximately a factor of two lower than HD14956, and a factor of two higher than HD13854. These two stars have been classified in Paper I as “highly processed” in that they are amongst the group of Galactic supergiants that show the highest N/C line strength ratios. The line strengths of Sher 25 are comparable to stars in this category, and the abundances we derive place it intermediate between HD14956 and HD13854 in terms of N enrichment. However it is certainly not extreme in its nitrogen abundance. It has a much higher abundance than HD2905, however we chose this star as a comparison specifically because it was one of the objects in Paper I with the lowest apparent N enrichment. This illustrates the wide variation in nitrogen abundances that is seen amongst early B-type supergiants, and the abundance in Sher 25 is similar to those Galactic stars which appear most N enhanced.

Lamers et al. (2001) have presented the envelope abundances that are predicted by the models of Meynet et al. (1994) after convective mixing in the red supergiant phase. This depends critically on two factors. Firstly it depends on the mass-loss during earlier phases, which is dominated by radiatively driven winds while the star is hot. Clearly the higher the mass-loss, the more of the envelope is lost and hence there is less gas of initial composition to mix with the CNO-processed core material. Secondly it will depend on how far into the core the convection reaches and how much core gas actually gets dredged up into the convective atmosphere. Lamers et al. (2001) have plotted the N/O and N/C ratios for various values of mass-loss rates and initial stellar mass. We estimate the zero-age main-sequence mass of Sher 25 to have been $60M_{\odot}$ from comparison with the Meynet et al. tracks in Fig. 6. Although we have directly derived a mass-loss rate for Sher 25 in its present status as a luminous B-type supergiant, it may have had a higher \dot{M} when it was a main sequence star. A $60M_{\odot}$ star on the main-sequence would have a mass-loss rate of typically $\sim 2 - 5 \times 10^{-6}M_{\odot} \text{ yr}^{-1}$ (Puls et al. 1996), hence during its H-burning lifetime (4 Myrs; from the Geneva models) it would have lost 8-20 M_{\odot} of its envelope through its stellar wind. The surface N/O and N/C ratios show a steep dependence on \dot{M} in this range, and the Lamers et al. calculations indicate ranges of $3 \lesssim \text{N/O} \lesssim 20$ and $6 \lesssim \text{N/C} \lesssim 30$.

In order to compare this meaningfully with the abundance ratios we derive, we must have confidence in the absolute abundances derived in our methods. To date the evaluation of this has been difficult, as pointed out in Smartt et al. (2001a, 1997) and Paper I. These studies have concentrated on differential analyses and comparisons of the difference between stellar subgroups, rather than assuming validity of the absolute abundances. In particular the absolute value of the carbon abundance in our stars is of dubious validity, as we discussed in detail in Sect. 3.1.2. Hence we will not quantitatively compare the N/C ratios in our stars to those in the evolutionary models. However as discussed in Sect. 3.1.2 the N and O absolute results should be reliable enough to carry out a meaningful comparison, providing we consider the probable errors in the methods. In Table 6 the N/O fraction is listed for each star. Given the uncertainties in the individual abundances, these ratios are uncertain within a factor of approximately 3. For Sher 25, the observed N/O ratio (0.36) is much lower than that expected from the Lamers et al. (2001) calculation for a star which has undergone convective dredge in the red supergiant phase (3–20), even allowing for an uncertainty of 3 in our derived results. For the most nitrogen rich star in our sample HD14856 (of initial mass approximately $40M_{\odot}$) N/O is predicted to be greater than 2, compared with our estimate of 0.53. This also implies the observed N/O ratio is too low to be compatible with convective dredge-up having occurred. The global analysis of the large sample of B-type supergiants in Paper I implied that their CNO line ratios and estimated abundances were not consistent with them (or even a subset

of them) being post red supergiant stars. Our analysis of Sher 25 indicates that it has similar CNO abundances to the “highly processed” stars, but that it is not extremely nitrogen rich. This suggests that, despite the appearance of the nebula, the star has *not* undergone dredge-up and thus has not previously been a red supergiant.

4.2. Evolution direct from the main sequence

Although we see no strong evidence for a previous red-supergiant stage of Sher 25, the abundances do suggest that some form of CN and NO cycle processed gas has been mixed into the stellar atmosphere. The sample in Paper I indicates that there is a range in the CNO abundances in stellar atmospheres. This is consistent with rotationally induced mixing while the stars are main-sequence O-types and/or as they evolve off the main-sequence to the cooler surface temperatures that we presently see. In this case one would envisage a range of C/N and N/O ratios in the atmospheres due to the distribution of rotational velocities. Lamers et al. (2001) have also estimated the C/N and N/O surface abundances for massive stars that undergo rotationally induced mixing. They calculate the surface abundance ratios as a function of the mixing time τ_{mix} and find that their results agree well with the calculations from Heger & Langer (2000) and Maeder (1998) if $\tau_{\text{mix}} \simeq 1 - 3\tau_{\text{MS}}$ (where τ_{MS} is the main-sequence lifetime). Further they estimate that $\tau_{\text{mix}} = 2-4 \tau_{\text{MS}}$ is needed to account for their observed LBV nebular abundance ratios.

For a $60M_{\odot}$ star the N/O ratio in the atmosphere of a blue supergiant which has undergone rotationally induced mixing is in the range of $1 < \text{N/O} < 3$ if τ_{mix} is 2 – 4 times the main sequence lifetime. The value for Sher25 (N/O=0.36) is lower than these predicted values for $2 < \tau_{\text{mix}} < 4$, but is a factor of 3 higher than the expected initial value of N/O=0.12. Our measured value suggests that Sher25 has undergone less mixing than these models predict, although almost certainly some moderate amount of mixing has occurred to enhance the N abundance. This suggests a larger mixing time (i.e. greater than 2 – 4) is more appropriate for Sher25.

5. Conclusions and wider implications

5.1. Implications for the evolutionary status of blue supergiants

From our detailed abundance analysis of Sher 25 and comparison to evolutionary calculations we can find no clear evidence that the star was previously in a red supergiant phase. The CNO abundances we derive at its surface are similar to those in other Galactic B-type supergiants which show somewhat enhanced N/C and N/O abundance ratios. However the extent of this enhancement does not appear to be high enough to suggest the star dredged up CN and NO cycle equilibrium core gas during a cool supergiant phase. Even allowing for a large mass-loss rate during its main-sequence lifetime does not reconcile the

results, and the current wind properties of Sher 25 also indicate that it is a relatively “normal” B-type supergiant. Certainly this star sits comfortably in the largest sample of Galactic B-type supergiants yet analysed (Paper I and Paper II), in terms of its mass, atmospheric parameters, abundances and wind properties. It does appear to be similar to the group of supergiants which show the largest N/C line strengths, and hence N/C abundance ratios but our quantitative comparison of the N/O results are more compatible with it having undergone some form of rotationally induced mixing either during or just after its main-sequence phase.

The sample of Galactic A-type supergiants analysed by Venn (1995) shows evidence for the stars having undergone partial mixing of CN-cycled gas. However the abundances derived are not suggestive of the stars having been through a first dredge up and hence are unlikely to be post red supergiant objects. Venn concludes that these 5-20 M_{\odot} stars have evolved directly from the main-sequence. The Galactic B-type supergiants analysed in Paper I are of higher mass ($\sim 20\text{-}40M_{\odot}$), and the results are also not consistent with them having undergone a previous red supergiant evolutionary phase. The study of the abundances in the nebulae around LBVs (in the 40-80 M_{\odot} mass range) by Lamers et al. (2001) again suggests that they have not previously been red supergiants and that the nebulae are ejected during the blue supergiant phase. The chemical enhancements seen in these three cases are possibly all due to some form of rotation induced mixing, which will have some broad distribution based on initial rotational velocities and mass-loss rates.

We find that the blue supergiant Sher 25 is also very unlikely to have gone through a red supergiant phase. Compared to other B-type supergiants in the galaxy, its atmospheric chemistry and wind properties are not peculiar in any way. Its peculiarity stems from the existence of the striking circumstellar nebula. Lamers et al. (2001) have speculated that the nebulae around LBVs have been ejected in the blue supergiant phase, although what the mechanism actually responsible for this is open to some debate. Therefore in the Galaxy, there is no single blue supergiant or nebula surrounding a blue supergiant, which displays abundances consistent with the star having evolved through a previous red-supergiant phase. The idea that nebulae surrounding massive, evolved stars must have been ejected during the red supergiant phase does not appear to be supported by stellar analyses of blue supergiants shown here, in Paper I and in Lamers et al. (2001).

5.2. Comparison with SN1987A

The origin of Sher 25’s nebulae is thus not well understood. Brandner et al. (1997b) have estimated the dynamical age of both the equatorial ring and bi-polar lobes to be around 6600yr, and the total ionized gas to be between 0.3 – 0.7 M_{\odot} . The current mass-loss rate is much

too low to have had much impact on the mass of this material, as in 6600yr the mass of gas ejected in the current fast wind is $\sim 0.01M_{\odot}$. Brandner et al. (1997a, 1997b) have also speculated that the Sher 25 nebula is similar in morphology, mass, composition and kinematics to that now seen around SN1987A. The SN1987A nebulae was almost certainly there before explosion, obviously too faint and compact to have been detected on pre-explosion plates, suggesting the progenitor star Sk–69°202 was at a similar evolutionary state to Sher 25 (although somewhat lower mass). By implication our results then suggest that Sk–69°202 may never have gone through the red supergiant phase, but rather evolved directly from the main-sequence and ejected its circumstellar material during the blue supergiant phase.

The initial ejecta of SN1987A was studied by Fransson et al. (1989) with IUE and ratios of N/C $\simeq 7.8$ and N/O $\simeq 1.6$ were found. The latter is significantly more than that in the atmosphere of Sher 25 and could be compatible with the progenitor having had a previous red supergiant phase from comparisons with the Lamers et al. calculations. However the modeling of this emission line spectrum is problematic and uncertainties in N/O are probably of the order ± 1 . Three features of the SN1987A event have caused problems for theoretical models looking for a consistent explanation of the event; the relatively high temperature of Sk–69°202; the stellar ring around the SN (Wampler et al. 1990, and Jakobsen et al. 1991); and the chemical anomalies discussed by Fransson et al. (1989). The review by Podsiadlowski (1992) suggests that no current theory of the evolution of single stars can simultaneously cope with all three and that binary accretion (or merger model) is theoretically the most promising, especially with regard to the mechanism for ring formation. We find no evidence for radial velocity variations of Sher 25 (within the uncertainties of $\sim 7\text{ km s}^{-1}$) although the four 1200s exposures were taken back to back. We plan future velocity monitoring of this star to determine whether or not it is a binary system. In the wider picture the question of how many blue supergiants are supernova Type II progenitors is very uncertain although new projects with data mining and the rich data archives which now exist may shed some light on this in the future (e.g. Smartt et al. 2001b). It would be also worthwhile to determine the CNO abundance ratios in other early B-type supergiants in the LMC in order to gain insight into the stars of similar metallicity at a similar evolutionary state to Sk–69°202.

Acknowledgements. Spectroscopic data were obtained at the Anglo-Australian Observatory in Siding Spring, New South Wales and we are grateful to the AAO staff for their assistance. We made use of the SIMBAD database maintained at CDS, Strasbourg. S. Smartt thanks PPARC for support through an Advanced Research Fellowship award. F. Rosales and N. Wright acknowledge PPARC support for the International Undergraduate Summer School held at the University of Cambridge during June and July 2001, during which time this work was carried out. We specially thank Margaret Penston for her efforts in organising this Summer school. We thank the

two referees Antonella Nota and Henny Lamers for their helpful comments.

References

- Brandner W., Grebel E.K., Chu Y.H. & Weis K., 1997a, *ApJ* 475, L45
- Brandner W., Chu Y.H., Eisenhauer F., Grebel E.K. & Points S.D., 1997b, *ApJ* 489, L153
- Butler K., 1984, Ph.D. Thesis, University of London
- Crowther P.A. & Dessart L., 1998, *MNRAS*, 296, 622
- Dennissenkov P. A., 1994 *A&A* 287, 113
- Deutschman W.A., Davis R.J. & Schild R.E., 1976, *ApJ Supp.* 30, 97
- Drissen L., Moffat A.F.J., Walborn, N.R. & Shara, M.M., 1995, *AJ* 110, 2235
- Eber F. & Butler K., 1988, *A&A* 202, 153
- Fransson C., Cassatella, A., Gilmozzi R. et al., 1989, *ApJ* 336, 429
- Gies D. R. & Lambert D. L., 1993, *ApJ* 387, 673
- Giddings J. R., 1981, Ph.D. Thesis, University of London
- Gilmozzi, R., Cassatella, A., Clavel, J., Gonzalez, R. & Fransson, C., 1987, *Nat* 328, 318
- Goss W.M. & Radhakrishnan V., 1969, *Astrophys. Lett.* 4, 199
- Grevesse N. & Sauval A.J., 1998, *Sp. Sci. Rev.*, 85, 161
- Heger A. & Langer N., 2000, *ApJ* 544, 1016
- Howarth I.D., Murray J., Mills D. & Berry D.S., 1998 *Starlink User Notice*, No.50.21
- Hubeny I., 1988, *Computer Physics Comm.*, 52, 103
- Jaschek M. & Jaschek C., 1967, *ApJ* 150, 355
- Kilian J., 1992, *A&A*, 262, 171
- Kudritzki, R.P., Puls, J., Lennon, D.J., et al., 1999, *A&A* 350, 970 (Paper II)
- Jakobsen P., Albrecht R., Barbieri C., et al., 1991, *ApJ* 369, L63
- Lennon D.J., Dufton P.L., Keenan F.P. & Holmgren D.E., 1991, *A&A*, 246, 175
- Lennon D.J., Dufton P.L. & Fitzsimmons A., 1993, *A&AS*, 97, 559
- Lennon D.J., 1983, *MNRAS*, 205, 829
- Lamers H.J.L.M., Nota A., Panagia N., Smith L.J. & Langer N., 2001, *ApJ* 551, 764
- Langer N. & Maeder A., 1995, *A&A* 295, 685
- Maeder A. & Meynet G., 2001, *A&A* 373, 555
- Maeder A., in *ASP Conf. Ser.* 131, *Boulder-Munich II: Properties of Hot Luminous Stars*, ed. I.D. Howarth, 85
- Meynet G., Maeder A., Schaller G., Schaerer D., & Charbonnel C., 1994, *A&AS*, 103, 97
- McErlean N. D., Lennon D. J. & Dufton, P. L., 1999, *A&A*, 349, 553 (Paper I)
- Melnick J., Tapia M. & Terlevich R., 1989, *A&A* 213, 89
- Moffat A.F.J., 1983, *A&A* 124, 273
- Podsiadlowski P., 1992, *PASP*, 104, 717
- Pandey A.K., Katsuo O. & Sekiguchi K., 2000, *PASJ*, 52, 847
- Puls J., Kudritzki R.-P., Herrero A., et al., 1996, *A&A* 305, 171
- Rolleston W.R.J., Smartt S.J., Dufton P.L. & Ryans R.S.I., 2000, *A&A* 363, 537
- Santolaya-Rey E., Puls J., & Herrero A., 1997, *A&A*, 323, 488
- Seaton M.J., 1979, *MNRAS* 187, 73
- Schaller G., Schaerer D., Meynet G., & Maeder A., 1992, *A&AS* 96, 269
- Sher D., 1965, *MNRAS* 129, 237
- Sigut T.A.A., 1996, *ApJ* 473, 452
- Smartt, S.J., Crowther P.A., Dufton P.L. et al. 2001, *MNRAS*, 325, 257
- Smartt S.J., Gilmore G.F., Trentham N., Tout C.A. & Frayn C.M., 2001, *ApJ* 556, 29
- Smartt S.J., Dufton P.L. & Lennon D.J., 1997, *A&A*, 326, 763
- Smartt S.J. & Rolleston W.R.J., 1997, *ApJ*, 481, 47
- Talon S., Zahn J.-P., Maeder A. & Meynet G., 1997, *A&A* 322, 209
- van den Bergh S., 1978, *A&A*, 63, 275
- Venn K.A., 1995, *ApJ*, 449, 839
- Vrancken M., Lennon D.J., Dufton P.L. & Lambert D.L., 2000, *A&A*, 358, 639
- Walborn N.R., Prevot M. L., Prevot L., et al. 1989, *A&A*, 219 229
- Walborn N.R., 1972, *AJ* 77, 312
- Wampler E.J., Wang L., Baade D., et al., 1990, *ApJ*, 362, L13